Bimodal Orientation Defects in Main-Chain Thermotropic Liquid Crystalline Polymer Fibers

ARTICLE *in* MACROMOLECULES · JANUARY 2002

Impact Factor: 5.8 · DOI: 10.1021/ma010731z

Bimodal Orientation Defects in Main-Chain Thermotropic Liquid Crystalline Polymer Fibers

Jennifer E. Taylor,[†,§] Angel Romo-Uribe,[‡] and Matthew R. Libera*[,†]

Department of Chemical, Biochemical, and Materials Engineering, Stevens Institute of Technology, Hoboken, New Jersey 07030, and Ticona (Celanese AG), 86 Morris Avenue, Summit, New Jersey 07901

Received April 27, 2001; Revised Manuscript Received November 14, 2001

ABSTRACT: The molecular orientation in as-spun fibers of main-chain thermotropic liquid crystalline polymers (TLCP) has been investigated using electron diffraction at high spatial resolution. Although a large degree of macromolecular alignment with the fiber axis is expected due to the large shear stress and elongational flow associated with the spinning process, a microdefect structure with a characteristic length on the order of 100−200 nm has been revealed. The microdefect structure consists of a bimodal orientation where macromolecules are aligned along two different directions. In some cases, the macromolecular orientation is nearly orthogonal to the fiber axis. The defect structure is not observed in heat-treated fibers, and the macromolecular orientation after heat treatment is rather uniform along and across the fiber. These results are consistent with the hierarchical structure of highly oriented liquid crystalline polymers observed by Sawyer and Jaffe [*J. Mater. Sci.* **1986**, *21*, 1897−1913] and add further insight into the hierarchical defect structure of highly oriented liquid crystalline polymers.

Introduction

Liquid crystalline polymers (LCP) continue to be the focus of intense study, because they possess anisotropic properties[1] that can be exploited for a multitude of load-bearing applications.[2,3] Thermotropic LCP's are used for high-performance fibers[4] and composite reinforcement[5] where exceptional strength and stiffness are greatly dependent on the perfection of molecular alignment. Parallel alignment of the molecules with the fiber axis is necessary at all length scales, so the strong covalent bonds within the molecules, rather than the weak secondary bonds between the molecules, bear the load.[6] Processing techniques to align the molecules with the fiber axis have been developed[6] and are effective on macroscopic length scales.

Critical to the process of deriving the best mechanical properties from the fibers is the ability to evaluate the degree of molecular alignment with the fiber axis. This alignment must be determined at length scales comparable to those associated with structural changes within the fiber.[7] Structural gradients across LCP fiber have been well documented[8−10] and indicate that the orientation is dependent in part on the spatially dependent shear stresses within the fiber during processing. A skin-core effect, where the molecular alignment at the outer surface is far better than at the center of the fiber, has been observed by selected-area electron diffraction and optical microscopy techniques in both thermotropic[10] and lyotropic[11] LCP's. A process yielding fibers with maximum molecular orientation and no variation in degree of alignment from skin to core is desired to fully exploit the mechanical properties of LCP for high strength applications.

A measure of the degree of molecular orientation in heat-treated fibers can be found through the determination of orientational order parameters.[12,13] These values are between 0 and 1 where the former corresponds to an isotropic state, and the latter indicates perfect molecular alignment with the fiber axis. X-ray[14] and neutron scattering,[15] among other techniques,[16] have been used to calculate orientation parameters. These values enable the determination of the local directors. Each director is a vector that has a length equal to the orientational order parameter and a direction corresponding to the average molecular orientation. In-situ X-ray diffraction studies have shown the molecular orientation response of thermotropic[14,17] and lyotropic[18] LCP under shear and during fiber spinning, respectively. A complementary postprocessing technique employing electron diffraction has been developed to resolve the degree of molecular alignment at submicron length scales.[19,20] The advantage of using this electron-optical technique is that electrons can be focused to sample submicron areas of specimen, thus alleviating structural averaging associated with the poorer spatial resolution of other techniques.

The rheological behavior of thermotropic LCP[14,17,21−25] in flow is atypical when compared to common thermoplastics. Although the polymer is nematic in the melt, domains of similarly aligned molecules are randomly arranged so the overall molecular orientation is isotropic. Unlike common thermoplastics, the molecules align either parallel ("flow-aligning") or perpendicular ("tumbling" or "log-rolling") to the velocity axis of flow, depending on conditions of temperature,[25] strain rate,[14] and molecular weight.[17]

In both thermoplastics and thermotropic LCPs, the degree of orientation is a function of processing conditions. Among the important factors affecting orientation are temperature, stress, die design, and draw down. Differences in local shear stress produce skin-core effects, where the molecular orientation within the center of the fiber is different from the outer layer.[26] During fiber-spinning of many thermoplastics, an amorphous outer layer is formed due to the freezing-in of the tangled molecular chains. Since the thermotropic LCP studied here consists of molecular chains that are both

† Stevens Institute of Technology.
‡ Ticona (Celanese AG); presently with Rohm and Haas, Springhouse, PA.
§ Presently with Cambridge University, UK.
* Corresponding author: fax (201) 216-8306; e-mail mlibera@stevens-tech.edu.

10.1021/ma010731z CCC: $22.00
Published on Web 01/22/2002

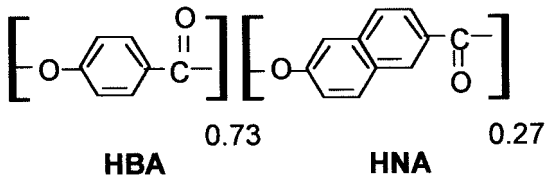

Figure 1. Chemical structure of 73 mol % 1,4-hydroxybenzoic acid and 27 mol % 2,6-hydroxynaphthoic acid.

straight and rigid, the molecules easily slip past each other in the highly stressed outer layer while the molecules in the center experience less shear stress and therefore are less well oriented.

The fiber-spinning process involves two melt-flow conditions: a capillary shear flow and an elongational flow of melt draw-down in a nonisothermal environment. The molecular orientation is mostly induced by elongational flow. Calundann and co-workers, for example, have shown that fiber-spinning processes of high-performance TLCP involve high shear rates on the order of 10^4 s^{-1} and draw-down ratios greater than 10.[27] Furthermore, Calundann et al. also demonstrated that increasing the drawn-down reduces the fiber diameter but does not increase the molecular orientation. Therefore, one can expect that the molecular chains are highly aligned with the fiber axis under those processing conditions.

The goal of this research is to spatially resolve the morphology and local orientation in an as-spun LCP fiber and then to assess the effect of heat treatment on the submicron molecular orientation. The electron-optical technique used here is necessary for the determination of submicron molecular alignment that is otherwise averaged out using conventional scattering techniques.[19] Maps are formed that are composed of two-dimensional arrays of vectors aligned along the average molecular orientation found from the spatially resolved diffraction patterns. Structural gradients are determined at submicron length scales by relating the vectors to the location in the fiber from which the diffraction patterns are collected. Through this technique, changes in the submicron molecular alignment are related to real-space images of the as-spun and heat-treated fibers. The new scientific information in this paper is that we find a bimodal orientation distribution at length scales on the order of 100 nm in a melt-processed fiber subjected to extremely high shear and elongational flow.

Experimental Section

Materials. Vectran (Vectran is a trademark of Celanese) fibers ~18 μm in diameter were supplied by Ticona (formerly Hoechst Celanese). The fibers were made of the wholly aromatic copolyester (Figure 1) composed of 73 mol % 1,4-hydroxybenzoic acid (HBA) and 27 mol % 2,6-hydroxynaphthoic acid (HNA). The as-spun fibers were heat-treated by Ticona in an inert atmosphere under tension. The heat treatment consisted of heating the fibers to 270 °C and holding the temperature for periods of 4−20 h.

Spatially Resolved Electron Diffraction. Samples for transmission electron microscopy were prepared by embedding the fibers in Epon 812 epoxy and cutting longitudinal slices by room temperature microtomy as shown in Figure 2. In order to be able to distinguish between intrinsic microstructural features and artifacts from the microtomy, the cutting was done at an angle 45° from the fiber axis. No interaction between the epoxy and LCP fibers was observed. Sections ~100 nm thick were placed on copper TEM grids covered by holey carbon support films. A Philips CM20 field emission gun (FEG) transmission electron microscope was used to collect

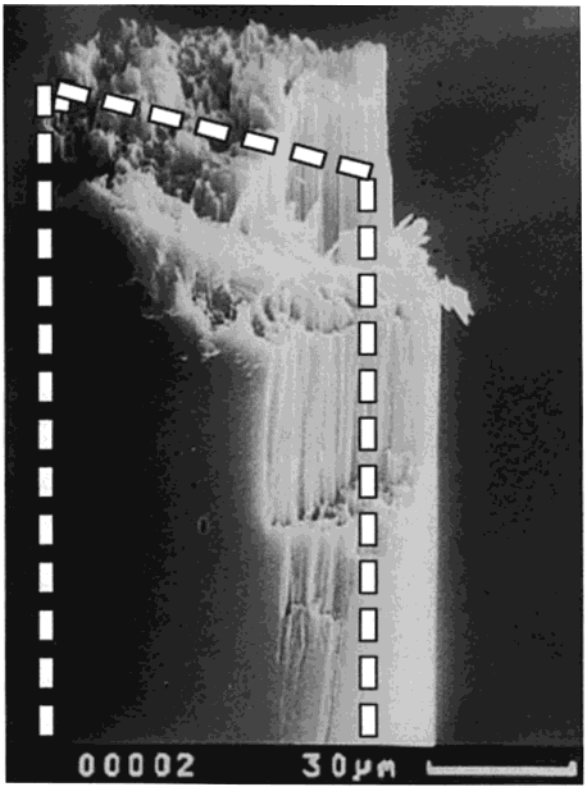

Figure 2. SEM image showing a heat-treated HBA/HNA fiber. This is a larger diameter fiber than those studied throughout the rest of this paper. The dotted line indicates a typical section and orientation from which thin TEM sections were cut.

electron diffraction patterns. Digital data were collected using a Gatan 694 slow scan CCD camera interfaced to the microscope. Gatan's Digital Micrograph software was used to digitally control the $x-y$ scan coils through the microscope's serial port as described elsewhere.[20] A script was written to control the interpixel spacing between points irradiated by the electron beam. The system was set to collect diffraction data as the electron probe was systematically moved across the sample as shown in Figure 3. The size of the radiative beam was manually set to be smaller than the interpixel spacing. The minimum area that could be confidently irradiated by the electron beam was found by determination of the critical dose for each polymer.[19,28]

Data Analysis. Intensity values from the digital diffraction patterns were extracted using several scripts. As shown in Figure 4a, the azimuthal angle of the equatorial peak was found to establish the direction of molecular orientation. The patterns were rotated so the maximum of the equatorial peak was at the vertical (90°). A script was used to acquire azimuthal traces of the intensities between 0° and 360°. The azimuthal intensity traces were collected at a diffracted radius q, which corresponds to the reciprocal space distance from [000] to the maximum equatorial peak at (Figure 4b). Orientational order parameters were calculated from diffraction patterns of heat-treated fibers using a procedure similar to that used for X-ray diffraction.[12,29] The diffracted intensity at 0° was subtracted from each set of azimuthal intensities to eliminate contributions of inelastic scattering to the calculated orientational order parameter. Additionally, intensity due to scattering from the amorphous carbon ligaments in the support film was eliminated by this background subtraction. Previous application of electron diffraction to calculate orientational order parameters in LCP fibers has shown that the intensity values must be corrected for relatively low signal-to-noise ratio and convergence angle between experiments.[19] However, correction for these factors is not considered in the present research, since orientation parameters were measured from diffraction patterns collected under the same experimen-

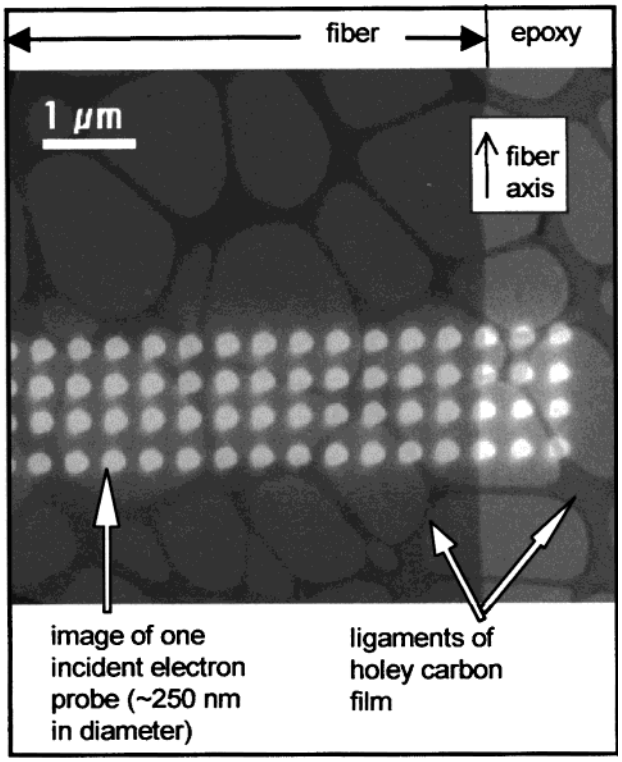

Figure 3. Bright-field image of heat-treated HBA/HNA fiber with the superimposed images of the electron probes (bright disks) used to collect spatially resolved diffraction data.

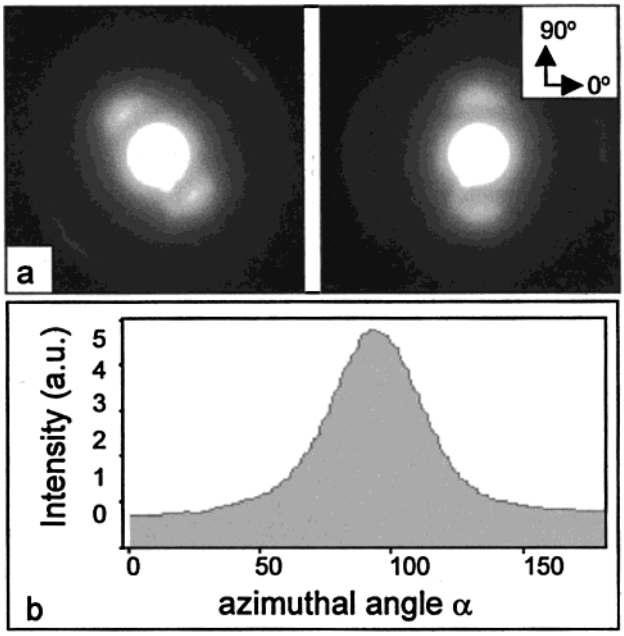

Figure 4. (a) Diffraction pattern obtained from heat-treated HBA/NA fiber. The pattern is rotated so the equatorial peak maximum is vertical. (b) Azimuthal intensities extracted from diffraction pattern in (a).

tal conditions for each set of data. Omitting these corrections leads to a systematic error, which does not affect conclusions drawn when comparing the results of different experiments performed identically.

Results

Diffraction patterns from as-spun and heat-treated fibers are shown in Figure 5a,b. These data were collected from an area 2.5 μm in diameter. The pattern

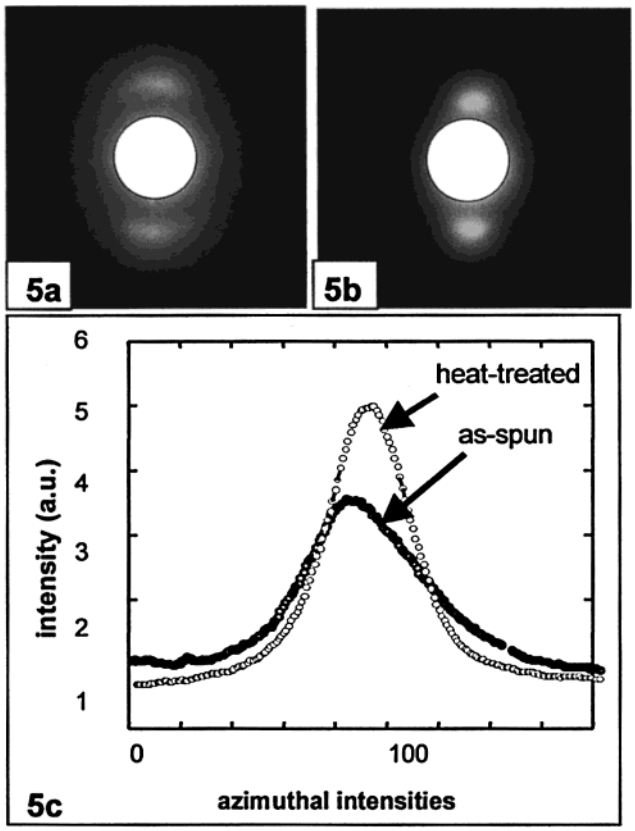

Figure 5. Diffraction patterns from (a) as-spun and (b) heat-treated HBA/HNA fibers. (c) Azimuthal intensities through main interchain equatorial maxima. Transmitted beam is blocked to accentual the equatorial reflections.

from the heat-treated fiber has more intense and concentrated equatorial reflections. The narrower spread in the radial direction shows that there is better interchain packing among the macromolecules. After background subtraction, a pseudohexagonal and orthorhombic phase[30,31] is evident in the as-spun and heat-treated fibers, respectively. Figure 5c shows normalized azimuthal intensity traces through the main interchain maxima for both fibers. Since the azimuthal spread is a measure of the degree of molecular orientation along the preferred direction (i.e., fiber axis), the heat-treated fiber shows narrower azimuthal intensity and therefore a greater average degree of molecular orientation.

Figure 6 shows a diffraction pattern acquired using an electron beam ~150 nm in diameter. This area is much smaller than the areas used to acquire the diffraction patterns in Figure 5. Strikingly, the pattern displays four reflections of which two pairs are separated by an azimuthal angle $\alpha = 77°$. The position of these reflections corresponds to $q = 1.4$ Å^{-1}, where q is the scattering vector ($4\pi \sin \theta/\lambda$), and therefore they are interchain equatorial reflections. Figure 6 also shows the azimuthal intensity trace through these maxima. It indicates clearly the position of the equatorial maxima. The pattern demonstrates that there is a bimodal orientation within the fiber at ~150 nm length scales. Thus, in this particular case, the average direction of each dominant orientation is 3° and 74° with respect to the fiber axis. This finding was typical of many regions sampled at a spatial resolution over 150 nm.

A bimodal phase indicating two distinct macromolecular orientations is seen in the as-spun fibers when areas sampled by the incident electron beam are on the

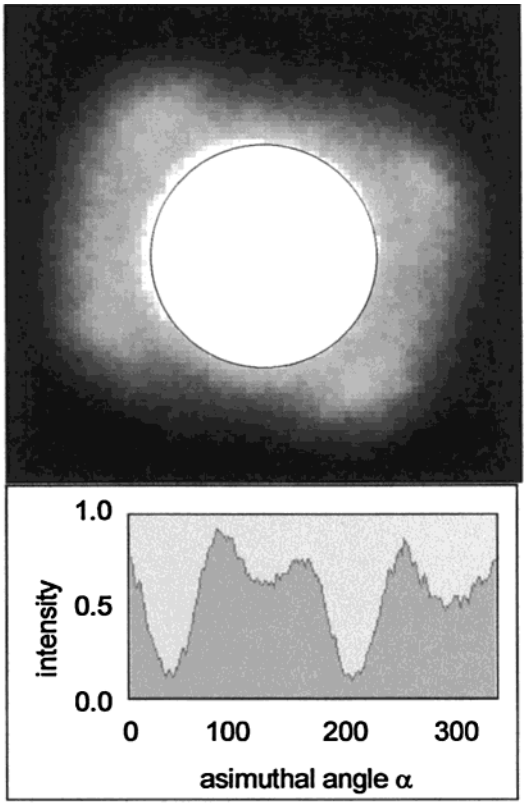

Figure 6. Electron diffraction patterns of as-spun HBA/HNA fiber. Azimuthal intensity profile shows that the equatorial peak splits indicating bimodal orientation.

order of 400 nm in diameter and smaller. Figure 7 shows a bright-field image of an as-spun fiber where images of the electron probes have been superimposed to show the size and location of the sampled areas. Azimuthal traces shown below the fiber image clearly indicate that the bimodal phase can be resolved when the spatial resolution is increased from 2.5 μm to 200 nm in diameter. Important to note is that the width of the set of equatorial peaks shown at 200 nm resolution is equal to the width of the single equatorial reflection from the 2.5 μm diameter sampled areas. This result then demonstrates the effect of structural averaging associated with other techniques such as X-ray and neutron scattering that have spatial resolution limitations on the order of microns.

To map molecular orientation in two dimensions, a series of diffraction patterns were collected from positions across the as-spun fibers. The directions of the dominant orientations, as determined by the position of the peak maxima of the bimodal equatorial reflections, are shown in Figure 8. The sampled areas are approximately 250 nm in diameter. A variation in the separation angle between sets of equatorial peaks is observed across the fiber. A single vector indicates that one direction of orientation is present. As shown in the inset, the molecular orientations in some regions of the fiber are almost perpendicular to the fiber axis. This is a feature associated with neither the skin nor the core of the fiber.

Figure 9 shows a bright-field TEM image of a heat-treated fiber. The molecular orientation was also mapped using the spatially resolved electron diffraction technique, and the corresponding vector maps are superimposed on this image. The size of the areas from which these diffraction patterns were collected is 100 nm in

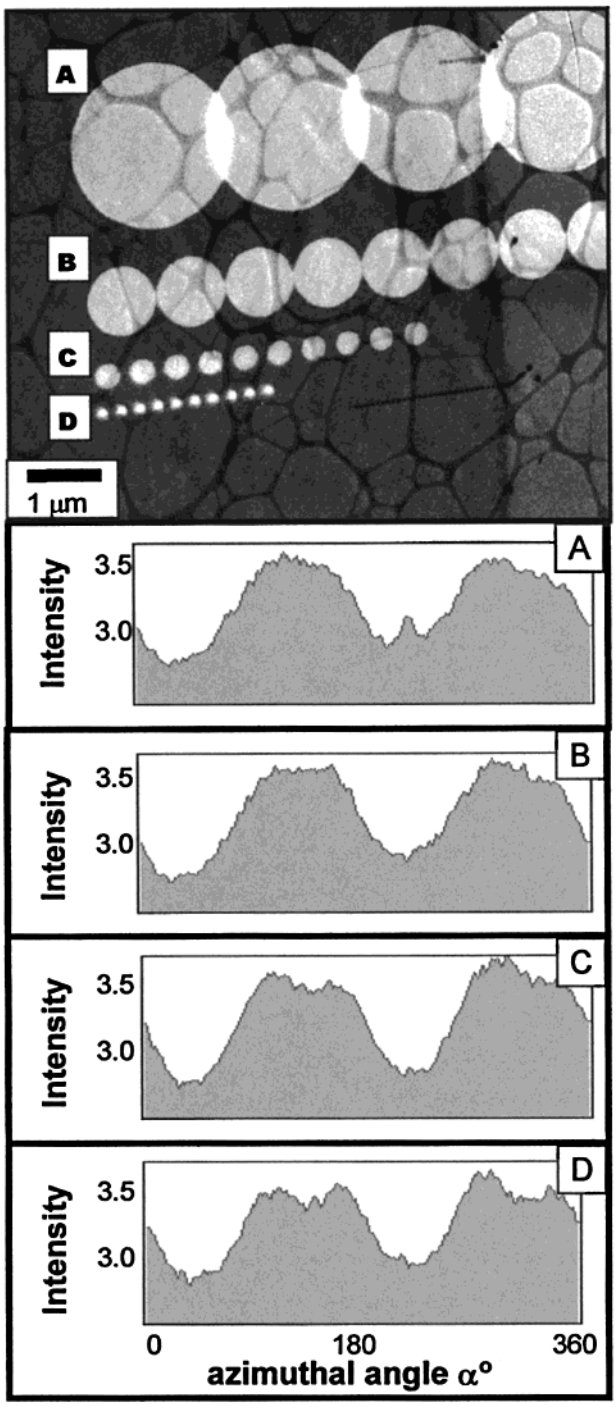

Figure 7. Top figure shows a bright-field image of an as-spun fiber with superimposed electron diffraction probes. Figures below are azimuthal scans from sampled areas above.

diameter. The results show that, at this resolution, the average macromolecular orientation is unimodal. Furthermore, little change in the magnitude or direction of the orientation vectors is found, thus indicating that the degree of orientation is relatively uniform across the area sampled. However, the vectors near the edge are slightly shorter than those at the interior of the fiber. Nevertheless, random sampling on other heat-treated fibers showed that there is no evidence of a bimodal orientation within these fibers.

Discussion

The enhanced spatial resolution of the technique used here has enabled us to investigate the microstructure

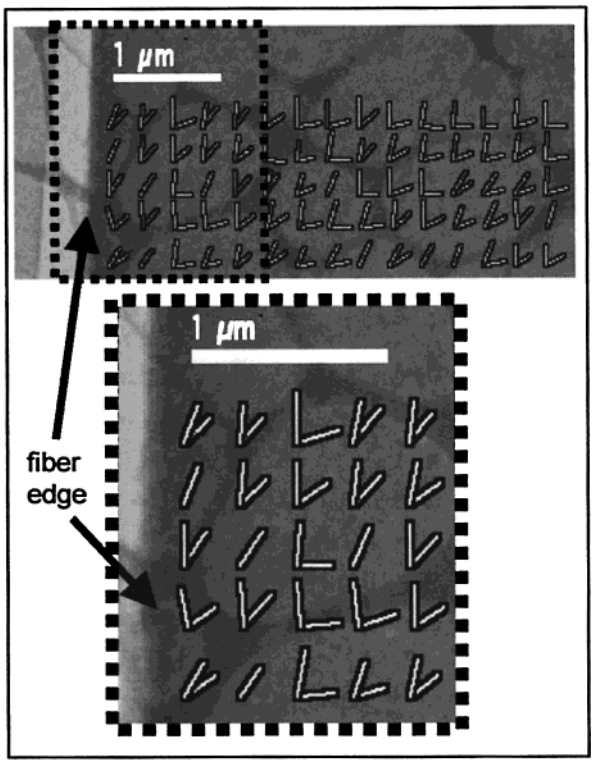

Figure 8. Vector map showing direction of molecular orientation in an as-spun fiber. Two vectors correspond to a bimodal orientation. Single vectors indicate unimodal orientation.

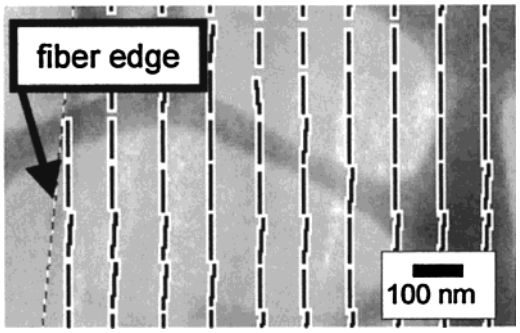

Figure 9. Bright-field image of heat-treated HBA/HNA fiber with superimposed orientational vector map.

of LCP fiber at submicron resolution. A distribution of molecular orientation is observed in as-spun fibers where the average molecular alignment varies from parallel to almost orthogonal with respect to the fiber axis, as shown in Figure 8. Wide-angle X-ray scattering (WAXS) has shown that the molecular orientational order parameters for as-spun fibers are on the order of 0.83.[19] Clearly, the magnitude of this value represents the average distribution of orientations existing within the fiber. The morphology revealed by the electron diffraction patterns is unexpected considering the stringent conditions of the fiber-drawing process. The liquid crystalline polymer has been subjected to contraction flow through a spinneret with a diameter of ~180 μm, shear rates on the order of 10^4 s^{-1}, and further extensional flow with a draw-down ratio on the order of 10.[1,27]

The bimodal phase observed in the as-spun fiber (Figure 7) arises from distinctly different molecular alignments. Sawyer and co-workers[10,32,33] have reported a hierarchical structure in LCP fibers. The hierarchy consists of macrofibrils of ~5 μm in diameter, fibrils of ~500 nm across, and microfibrils of the order of ~50 nm wide and 5 nm thick. Furthermore, these authors have also suggested the existence of a defect hierarchy inherent to the LCP structure. The term defect hierarchy is meant to describe deviations from a rodlike behavior along the molecular axis. When the spatial resolution in the present experiment is increased to ~400 nm or less in diameter, the equatorial reflections start to split, revealing nonuniformity in the molecular alignment. This observation therefore suggests that the bimodal diffraction patterns arise from contributions of the microfibrils (~50 nm in diameter) contained within the fibrils (~500 nm in diameter).

The large separation angles between dominant orientations of the bimodal alignments represented in the vector map of Figure 8 suggest a tortuous path of the molecular chains along the fiber axis. However, important to realize is the significant effect of the spatial resolution afforded by the electron diffraction technique used here on the description of molecular correlation. The HBA/HNA copolyester has an average contour length per monomer length, l_0, of 0.686 nm, an average molecular weight per monomer unit (M_w^{mono}) of 135 g/mol, and a hydrodynamic cross section of ~0.6 nm. Therefore, a copolymer of molecular weight (M_w) 30 000 g/mol has a contour length, $l_c = l_o(M_w/M_w^{mono})$, of ~150 nm. By this calculation, the vector map at a resolution of 250 nm in diameter averages the orientation of approximately 2 molecular chains end to end, if full extension of the macromolecules is assumed, and 417 molecules across the area sampled by the electron probe. On the other hand, the thickness of the specimen is ~100 nm, so there could be as many as 160 molecular chains lying upon one another. In view of these considerations, it is clear that in some cases the molecular orientation can be orthogonal to the fiber axis because there is no interchain connection between different regions. This scenario is also consistent with the hierarchical LCP structure described by Sawyer and coworkers.[10]

Examination of the heat-treated fibers shows that there is a uniform alignment with the fiber axis throughout the fiber (Figure 9). The uniform molecular alignment observed in the heat-treated fiber has its imprint on the overall molecular orientation, as shown by X-ray diffraction where the molecular orientational order parameter for this case is measured to be 0.93.[19] The fact that the macromolecular orientation becomes more precisely parallel to the fiber axis agrees with previous findings by Ward et al., who found that the molecular chains of heat-treated HBA/HNA fibers become more tightly packed along the *c*-axis.[34]

Heat treatment of HBA/HNA fibers produces a significant increase in tenacity and some increase in modulus. The resistance to solvents and high temperatures is also enhanced.[1,27] The results of the present research show that the improvement in mechanical performance may be attributed to the elimination of the microdefects[10] that have been observed throughout the fiber. Calundann and co-workers have also reported that during heat treatment the degree of crystallinity in the fiber remains constant, but the perfection of the crystallites improves. Because of the improved alignment of molecular chains observed in the heat-treated fibers, the likelihood of molecular sequence matching is greatly improved. This would account for the heightened perfection of crystallinity in the structure.

In comparing the morphology of as-spun and heat-treated fibers, the question remains of how the bimodal phase is eliminated during heat treatment. The heat treatment is carried out 20−30 °C below the melting transition. At this temperature, the molecular chains have enough energy to move locally around their positions. However, it is not clear how the macromolecules could rotate toward the fiber axis, particularly in the cases where the bimodal phase has a separation of almost 90°. The likelihood of reorientation being driven solely by thermal processes is low. The answer may be in the chemical experience of the macromolecules during heat treatment. Heat treatment significantly increases the molecular weight of as-spun fiber.[27] During this process, the fibers experience solid-state polymerization, where transesterification reactions are also involved.[31,35,36] Transesterification involves either a chain end reacting with part of a neighboring molecule to leave a new end or two adjacent chains swapping connections at one point. The improvement in molecular orientation along the fiber axis may arise from swapping of units between molecular chains and not from the full molecular rotation toward the fiber axis.

Conclusions

Spatially resolved electron diffraction has revealed the hierarchical microdefect structure in as-spun LCP fibers. The electron diffraction patterns at a resolution of 100−200 nm showed a complex molecular orientation in as-spun fibers where the predominant submicron orientation is bimodal. The ability to recognize this behavior is only apparent because of the high spatial resolution achieved. The broad distribution of orientations corresponds to the defect structure proposed by Sawyer et al.[10] Microdefects arise from the orientation of imperfectly aligned (along the fiber axis) molecular chains of the microfibrils contained within the fibrils. Strikingly, the analysis of heat-treated fibers showed a uniform molecular orientation along the fiber axis with no evidence of bimodality.

Acknowledgment. The authors thank Linda Sawyer of Ticona (Celanese AG) for providing the LCP fibers used in this research and for a significant contribution of time and valuable knowledge. Many thanks to Professor Michael Jaffe for sharing his superlative understanding of LCPs and fiber processing. This research was supported by the Army Research Office through Grants DAAG55-97-1-0137 and DAAG55-98-1-0150.

References and Notes

(1) Calundann, G. W.; Jaffe, M. *Proc. Robert A. Welch Con. Chem. Res.* **1982**, *26*, 247−291.
(2) Sawyer, L. C.; Linstid, H. C.; Romer, M. *Plast. Eng.* **1998**, *54*, 37−41.
(3) Applications in LCP Materials. Jansson, J. F. In *Liquid Crystal Polymers: From Structures to Applications*; Collyer, A. A., Ed.; Elsevier Applied Science: Cambridge, 1992; p 281.
(4) Orientation in Liquid Crystal Polymers, Mitchell, G. R.; Windle, A. H. In *Orientation in Liquid Crystal Polymers*; Bassett, D. C., Ed.; Elsevier Applied Science: Essex, 1988; p 115.
(5) Calundann, G.; Jaffe, M.; Jones, R. S.; Yoon, H. In *Fibre Reinforcements for Composite Materials*; Bunsell, A. R., Ed.; Elsevier Science: Amsterdam, 1988; p 211.
(6) Calundann, G. W.; Charbonneau, L. F.; Shepherd, J. P. *Makromol. Chem. Macromol. Symp.* **1991**, *51*, 147−152.
(7) Donald, A. M. *Philos. Mag. A* **1983**, *47*, L13−L17.
(8) Cakmak, M.; Teitge, A.; Zachmann, H. G.; White, J. L. *J. Polym. Sci., Polym. Phys.* **1993**, *31*, 371−381.
(9) Hsiung, C. M.; Cakmak, M. *Proc. Antec* **1991**, 1063−1070.
(10) Sawyer, L. C.; Jaffe, M. *J. Mater. Sci.* **1986**, *21*, 1897−1913.
(11) Dobb, M. G.; Robson, R. M. *J. Mater. Sci.* **1990**, *25*, 459−464.
(12) Mitchell, G. R.; Windle, A. H. *Polymer* **1983**, *24*, 1513−1520.
(13) Haase, W.; Fan, Z.-X.; Muller, H. J. *J. Chem. Phys.* **1988**, *89*, 3317−3322.
(14) Romo-Uribe, A.; Windle, A. H. *Macromolecules* **1996**, *29*, 6246−6255.
(15) Dadmun, M. D.; Han, C. C. *Macromolecules* **1994**, *27*, 7522−7532.
(16) Pirnia, A.; Sung, C. S. *Macromolecules* **1987**, *21*, 2699−2706.
(17) Romo-Uribe, A.; Windle, A. H. *Proc. R. Soc. London A* **1999**, *455*, 1175−1201.
(18) Reikel, C.; Dieing, T.; Engstrom, P.; Vincze, L.; Martin, C.; Mahendrasingam, A. *Macromolecules* **1999**, *32*, 7859−7865.
(19) Taylor, J.; Romo-Uribe, A.; Libera, M. *Polymer* **2002**, *43*, 1641−1648.
(20) Taylor, J.; Libera, M.; Greeley, M. *Mater. Res. Soc. Symp. Proc.* **1999**, *559*, 128.
(21) Romo-Uribe, A.; Windle, A. H. *Macromolecules* **1993**, *26*, 7100−7102.
(22) Romo-Uribe, A.; Windle, A. H. *Macromolecules* **1995**, *28*, 7085−7087.
(23) Romo-Uribe, A.; Mather, P. T.; Chaffee, K. P.; Han, C. D. *Mater. Res. Soc. Symp. Proc.* **1997**, *461*, 63−68.
(24) Romo-Uribe, A. *Proc. R. Soc. London A* **2001**, *457*, 207−229.
(25) Romo-Uribe, A.; Lemmon, T. J.; Windle, A. H. *J. Rheol.* **1997**, *41*, 1117−1145.
(26) Sawyer, L. C.; Jaffe, M. *Mater. Res. Soc. Symp. Proc.* **1992**, *255*, 75−85.
(27) Yoon, H. N.; Charbonneau, L. F.; Calundann, G. W. *Adv. Mater.* **1992**, *4*, 206−214.
(28) Spontak, R. J.; Windle, A. H. *Polymer* **1990**, *31*, 1395−1400.
(29) Deutsch, M. *Phys. Rev. A* **1991**, *44*, 3−9.
(30) Wilson, D. J.; Vonk, C. G.; Windle, A. H. *Polymer* **1993**, *34*, 227−237.
(31) Blackwell, J.; Schneider, A. I.; McCullagh, C. M. *Mater. Res. Soc. Symp. Proc.* **1994**, *321*, 71−80.
(32) Sawyer, L. C.; Chen, R. T.; Jamieson, M. G.; Musselman, I. H.; Russell, P. E. *J. Mater. Sci., Lett.* **1992**, *11*, 69−72.
(33) Sawyer, L. C.; Chen, R. T.; Jamieson, M. G.; Musselman, I. H.; Russell, P. E. *J. Mater. Sci.* **1993**, *28*, 225−238.
(34) Nicholson, T. M.; Ward, I. M. *Polymer* **1998**, *39*, 315−317.
(35) Hanna, S.; Romo-Uribe, A.; Windle, A. H. *Nature* **1993**, *366*, 546−549.
(36) Deak, D. K.; Lenz, R. W.; Kantor, S. W. *Macromolecules* **1999**, *32*, 3867−3874.

MA010731Z